

# The Effect of Corona Wire Position and Radius in a Duct-Type ESP with Wavy Collecting Plates

Angel G. Asipuela González, Mo'ath Bani Fayyad, and Iváncsy Tamás  
Budapest University of Technology and Economics/Electric Power Engineering, Budapest, Hungary  
Email: {gabriel.bme\_2020; mbanifayyad}@edu.bme.hu; ivancsy.tamas@vet.bme.hu

**Abstract**—Electrostatic precipitators (ESPs) have become one of the most effective methods for removing harmful particles from various industries. Many investigations in this subject are constantly developing due to the inherent benefits of using an ESP, and there are many robust initiatives taking place today all over the world. Different configurations of collection and discharging electrodes must be investigated to improve the ESP performance of ESPs. Many studies are working to enhance existing models in different ways. The geometry of the electrodes and the collecting plates is one area that could be improved. This paper investigates the wavy designs of collecting electrodes with varied corona electrode radius (range of variable corona radius (0.07-0.6 mm)) and position in a single-stage ESP. Wavy plates (WPs) and Inverted wavy plates (InvWPs) are compared to flat plates (FPs) using a numerical simulation tool. The results of this work show the impact of changing the corona radius when wavy and inverted wavy collecting electrodes are used on the electric potential, electric field strength, current density, and space charge density distribution, and particle collection efficiency. When compared to InvWPs and FPs, WPs show the highest performance in this range of particles. Although InvWPs can be utilized to reduce current density or space charge density, they do not increase particle collection efficiency.

**Index Terms**—ESP, space charge density, particle collection, particle charging, wavy collecting plates

## I. INTRODUCTION

Removing suspended particles from gases is one of the most fundamental observable and methodological challenges of the industrial era. Limiting emissions [1] by appropriate gas-cleaning techniques is critical for dealing with severe hazardous air pollution and, in many circumstances, for obtaining valuable materials such as copper, lead, or gold that would otherwise be conveyed up the flue and lost by dispersing into the atmosphere. ESPs had a total particle removal performance of up to 99 percent. The removal efficiency for fine particles, on the other hand, was relatively low [2]–[4].

The fine particles have a large specific surface area and could quickly overburden a variety of toxic and dangerous substances, posing a risk to human health [5], [6]. Fluid dynamics, corona discharge, particle charging,

and particle dynamics were all included in the operation of ESPs [5], [7]. The removal efficiency of fine particles in ESPs was experimentally investigated by Y. Zhuang *et al.* [2]. They focused on how particle collection efficiency in the cylindrical ESP is affected by gas velocity and electrical potential. The arrangement of collecting plates and corona discharges has a considerable impact on the collecting performance of the ESPs. As a result, many studies have been conducted to understand better and overcome the drawbacks of ESPs and modifying the shapes of the collecting plates and the discharge electrodes. Some experiments used a large dust collector to maximize removal efficiency based on the design of the ESP's collecting plates [8]. The impacts of wire-to-wire electrode distance and the wire to collecting plate distance on dust collection efficiency were investigated [5], [9]. Many numerical simulations have been carried out in order to explore different models of ESP collecting plates. Flat collecting plate (FP) and specific designs that are comparable to FP's have been used to analyze electrohydrodynamic (EHD) in ESPs [10]–[12]. Shen *et al.* investigated (EHD) in a wire plate ESP numerically [12], the flow patterns and corona electric fields were modified by arranging five different forms of collecting plates. In addition, numerical studies of the C-type collecting type [12] and the corrugated form [11] were conducted. Furthermore, Zhou *et al.* [13] examined a triangular form, W-type, and crenelated type. Still though, the wavy shape has been performed to examine electrical properties without affecting the space charge [14]. Regarding the impact of corona discharge electrodes on the efficiency of ESP, several experimental and analytical studies conducted by Jedrusik *et al.* [9], Gao *et al.* [15] examined the geometric properties of corona wires and ESP collection efficiency. The influence of ionic wind on the airflow field and particle precipitation was studied by Wang *et al.* [16] using a spike-honeycomb configuration. Some researchers have focused on various corona discharge electrode designs, such as barbed wire, which generate higher velocity and current density [15], [17].

On the other hand, several factors influence the efficiency of ESP depending on the corona electrode, including the effect of the number of discharge wires, whereas increasing the number of wires increases the corona current for the same voltage level [18], [19]. Besides that, the influence of wire-to-wire separation on the I-V characteristics of the ESP [20], [21] was investigated. Furthermore, wire radius has a substantial

Manuscript received November 15, 2021; revised January 20, 2022; accepted March 11, 2022.

Corresponding author: Angel G. Asipuela González (email: gabriel.bme\_2020@edu.bme.hu).

impact on the I-V characteristics of the ESP; for the same applied voltage, the total discharge current of lower-radius corona wires is higher than of high-radius corona wires [22]. However, these investigations were limited to ESPs with a fixed corona wire size. None of them investigated the wavy collecting plate with different sizes of corona discharge electrode. The present study aimed to show how changing the corona radius affected the operation of a wavy collecting plate and an inverted wavy plate (which was built as a reversed version of the wavy plate to examine the position of corona wires compared to the wavy plate). The impact of changing the radius of the corona electrode on the electric potential distribution, fluid flow velocity, electric field strength, current density, space charge density, particle trajectory motion, and collection efficiency when wavy and inverted wavy collecting plates are used.

## II. NUMERICAL MODEL

### A. ESP Numerical Methods Modeling

The numerical simulation was carried out using the properties listed in Table I; the study's goal was to use a pair of wavy collecting electrodes and different sizes of corona electrodes. Each study case has its 2-dimensional model.

TABLE I: SPECIFIC GEOMETRY FOR THE ESP ARRANGEMENT

Parameters used for simulation			
Parameter	Value	Parameter	Value
Length (mm)	700	Temperature (K)	293.15
Distance between two corona wires (mm)	150	Gas density $\text{kg}\cdot\text{m}^{-3}$	1.2
Distance between the collecting plates (mm)	100	Gas viscosity (Pa·s)	$2.57\times 10^{-7}$
Wave relation $A/s$	0.3	Pressure (atm)	1
Wavelength relation $\lambda/(2c)$	1	Particle diameter ( $\mu\text{m}$ )	0.01~5
Number of corona electrodes	3	Particle density $\text{kg}\cdot\text{m}^{-3}$	2200
Corona electrode radius (mm)	0.07~0.6	Particle relative permittivity	5
Applied voltage (kV)	20	Reduced Ionic mobility $\text{m}^{-1}\cdot\text{V}^{-1}\cdot\text{s}^{-1}$	$3\times 10^{21}$

### B. Corona and Collecting Electrodes Geometry

Corona electrodes have varying radiuses ranging from 0.07 to 0.6 mm. When wavy (WPs) and inverted-wavy (InvWPs) electrodes are being examined, flat collecting electrodes (FPs) are employed as a reference.

The collecting electrodes are at the top and bottom of the geometries in Fig. 1 and Fig. 2 whereas the corona electrodes are in the middle of the ESP. The fluid flow's inlet and outlet are specified on the left and right sides, respectively.

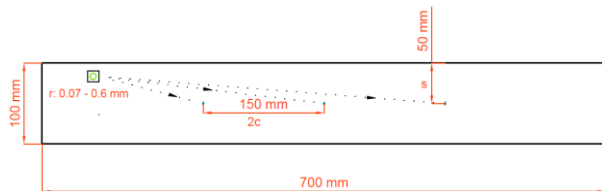


Fig. 1. Geometric configuration of flat collecting plates (FPs).

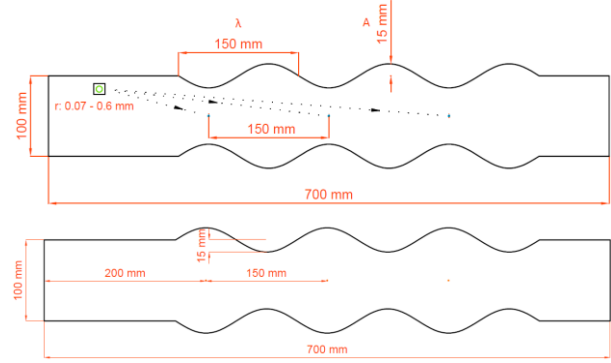


Fig. 2. Geometric configuration of wavy collecting plates (WPs).

The ESP length for the three types of collecting electrodes is 700 mm, the distance between the two corona electrodes is 150 mm, and the distance between the collecting electrodes is 100 mm; in the case of wavy electrodes the wave is defined by the relation of  $\lambda/2c=1$  and  $A/s=0.3$ , a prior research found that this geometric arrangement achieves the best efficiency with these connections [14].

The simulation is configured to perform at a temperature of 293.15 K and a pressure of 1 atm. The fluid flow is described as air and the characteristics of air, such as viscosity and density, are temperature and pressure dependent. With an average velocity of 1 m/s, an incompressible laminar flow is formed. The particle and air characteristics are specified in Table I. An electric potential of 20 kV is supplied to the corona electrodes for the simulation, while 0 V is provided to the collecting electrodes. The mesh is created using a normal triangle element size that has been optimized for fluid dynamics by the program.

### C. Electrostatics - Corona Discharge

Poisson's equation and the charge conservation equation have been used to characterize the corona discharge [23],

$$\partial \rho_q / \partial t + \nabla \cdot \mathbf{J} = 0 \quad (1)$$

$$\mathbf{J} = z_q \mu \rho_q \mathbf{E} + \rho u \quad (2)$$

$$\epsilon_0 \nabla^2 V = -\rho_q \quad (3)$$

$$\mathbf{E} = -\nabla V \quad (4)$$

where  $\rho_q$  ( $\text{C}\cdot\text{m}^{-3}$ ) is the space charge number density,  $\mathbf{J}$  ( $\text{A}\cdot\text{m}^{-2}$ ) is the current density,  $z_q$  is the charge number,  $\mu$  ( $\text{m}^2\cdot\text{V}^{-1}\cdot\text{s}^{-1}$ ) is the ion mobility,  $\mathbf{E}$  ( $\text{V}\cdot\text{m}^{-1}$ ) is the electric field,  $u$  ( $\text{m}\cdot\text{s}^{-1}$ ) is the fluid velocity,  $\rho$  ( $\text{kg}\cdot\text{m}^{-3}$ ) is the fluid density,  $\epsilon_0$  ( $\text{F}\cdot\text{m}^{-1}$ ) is the free-space permittivity, and  $V$  (V) is the electric potential [24].

Solving these equations provides the electric potential and the space charge density. Boundary conditions are required to achieve these solutions, one of them is defined by Peek's equation, which defines the electric field as a constant value on the corona electrodes ( $n\cdot\mathbf{E}=\mathbf{E}_0$ ). The other boundary conditions for Poisson's equation are ( $V=0$ ) at the collection plates and zero charge at the inlet and outlet [24], [25]:

$$\mathbf{E}_0 = 3 \times 10^6 \delta \left( 1 + 0.03 / \sqrt{\delta r_w} \right) \quad (5)$$

$$\delta = (T_0/T) \cdot (P/P_0) \quad (6)$$

where  $E_0$  ( $\text{V}\cdot\text{m}^{-1}$ ) is the electric field on the corona electrode,  $r_w$ (m) is the corona electrode radius,  $\delta$  is a relation between  $T_0$  (293.15°K) the absolute temperature and  $P_0$  (760 mmHg) the normal atmospheric pressure and  $P$  and  $T$  are the operating values.

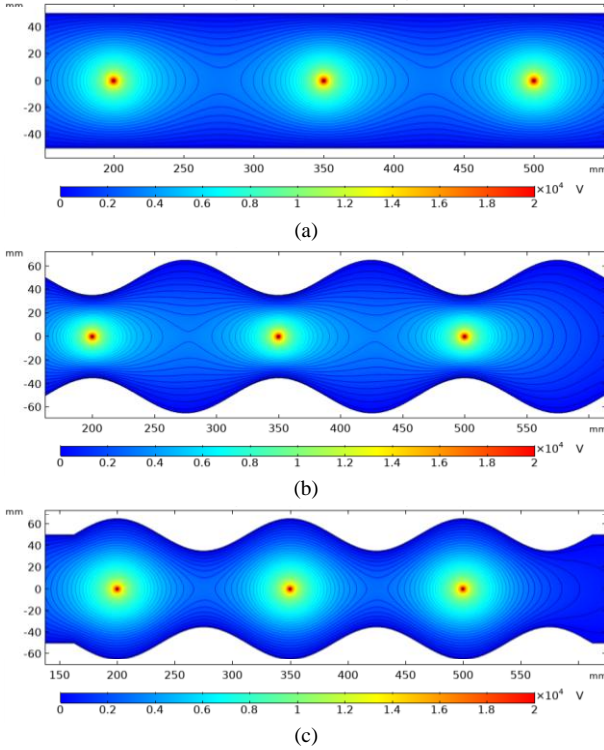


Fig. 3. Electric potential distribution using: (a) FPs, (b) WPs, and (c) InvWPs.

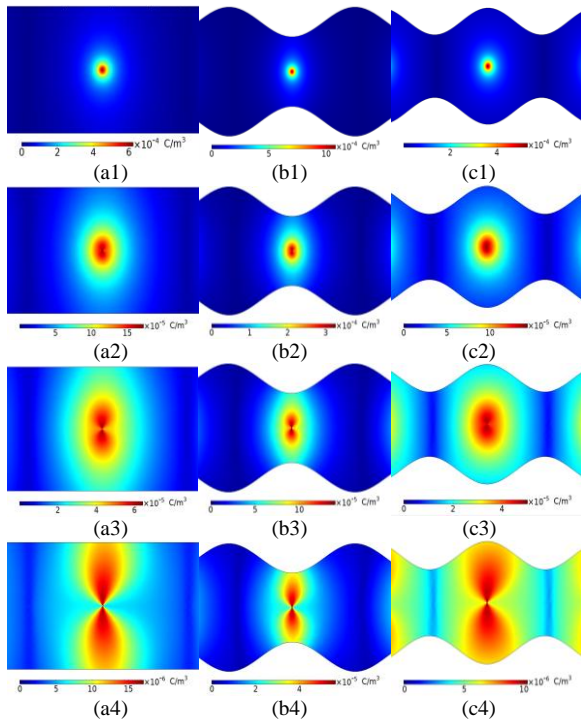


Fig. 4. Space charge density distribution with FPs(a), WPs(b), and InvWPs(c), and corona wire radius (a1) (b1) (c1) 0.07 mm, (a2) (b2) (c2) 0.24 mm, (a3) (b3) (c3) 0.42 mm, and (a4) (b4) (c4) 0.6 mm, respectively.

The electric potential distribution is shown in Fig. 3, for each case FPs, WPs, and InvWPs respectively. An electric potential of 20 kV is applied to the corona wires, and both collecting plates are set to ground. For this example, the corona wire radius is set to 0.5 mm.

The space charge density distribution for the different radius of corona wires with FPs, WPs, and InvWPs is shown in Fig. 4, where it was noticed that the space charge density distribution is symmetrical towards the collecting plates and increasing the radius of corona wire decreases the space charge density.

#### D. Fluid Flow

Navier-Stokes' equation (8), which is based on the conservation of mass and moment, defines and solves laminar fluid flow:

$$\rho \Delta \cdot u = 0 \quad (7)$$

$$\rho \frac{\partial u}{\partial t} + \rho (u \cdot \nabla) u = \quad (8)$$

$$\nabla \cdot [-pI + \mu(\nabla u + (\nabla u)^T)] + F_{\text{EHD}}$$

where  $\rho$  ( $\text{kg}\cdot\text{m}^{-3}$ ) is the fluid density,  $p$  (Pa) is the pressure,  $\mu$  ( $\text{kg}\cdot\text{m}^{-1}\cdot\text{s}^{-1}$ ) is the dynamic viscosity, and  $F_{\text{EHD}} = \rho_q E$  is the electrohydrodynamic force [24].

#### E. Particle Charging

In many circumstances, the particles exhibit an electronegative affinity; for example, when they enter an ionized field, they begin to trap ions until they reach a charge saturation threshold. Particle charging was classified into two mechanisms: field charging and diffusion charging, which were dominant for large and tiny particles, respectively. The Lawless model, which incorporated the two mechanisms, was used in this work [5], [24], [25]:

$$\tau_c \frac{dZ}{dt} = \begin{cases} \frac{v_s}{4\epsilon_0} \left(1 - \frac{v_e}{v_s}\right)^2 + f_a, & |v_e| \leq |v_s| \\ \frac{v_e - v_s}{\exp(v_e - v_s) - 1} f_a, & |v_e| > |v_s| \end{cases} \quad (9)$$

$$\tau_c = \frac{e^2}{4\pi\rho_q\mu k_B T_i} \quad (10)$$

where  $\tau_c$  is the charging time,  $Z$  is the charge number,  $k_B$  is the Boltzmann's constant, and  $T_i$  is the ion temperature, and

$$v_s = 3w_e \frac{\epsilon_{r,p}}{\epsilon_{r,p+2}} \quad (11)$$

$$v_e = \frac{Ze^2}{4\pi\epsilon_0 r_p k_B T_i} \quad (12)$$

$$w_e = \frac{er_p |E|}{k_B T_i} \quad (13)$$

where  $v_e$  is the self-potential of the particle,  $w_e$  is the electric field,  $\epsilon_{r,p}$  is the relative permittivity of the particles, and  $f_a$  is an analytic fitting function:

$$f_a(w_e) \equiv \begin{cases} \frac{1}{(w_e + 0.475)^{0.575}} & , w_e \geq 0.525 \\ 1 & , w_e < 0.525 \end{cases} \quad (14)$$

### F. Particle Kinetics

The trajectories that the particles travel until the collecting electrodes collect them may be described by Newton's second law while they are being charged by the ionized space and carried by the gas flow. There are two forces to consider: the drag force and the electric force caused by the flow and the electric field respectively:

$$\frac{dx(m)}{dt} = v, \quad \frac{d}{dt}(m_p v) = F_t \quad (15)$$

where  $x(m)$  is the particle position,  $v$  ( $m \cdot s^{-1}$ ) is the particle velocity,  $m_p$  (kg) is the particle mass, and  $F_t$  (N) is the total force on the particle.

The drag force  $F_D$  (N) is defined by equation (16), which includes rarefaction corrections defined by the Cunningham-Millikan-Davis model [24], and the electric force  $F_e$  (N) is described by equation (17):

$$F_D = \frac{1}{\tau_p S} m_p (u - v), \quad \tau_p = \frac{4\rho_p d_p^2}{3\mu C_D Re_r} \quad (16)$$

$$F_e = eZE \quad (17)$$

where  $\tau_p$  (s) is the particle velocity-time response;  $S$  is the drag correction coefficient,  $\rho_p$  ( $kg \cdot m^{-3}$ ) is the density of the particles;  $d_p$  (m) is the particle diameter;  $C_D$  is the Cunningham correction factor; and  $Re_r$  is the Reynolds number [2], [13],  $e$  (C) is an elementary charge and  $Z$  is the accumulated charge number on the particle [24].

### G. Particle Collection

There are models that may be used to compute the collection efficiency in a duct-type ESP based on its geometric design as well as the flow and particle velocities, including such Deutsch's equation, [26]:

$$\eta = 1 - \exp\left(-\frac{Lv}{su}\right) \quad (18)$$

Moreover, in this study, the collection efficiency is determined by counting the particles at the ESP output for a duct-type ESP and is defined by the length of the collecting plate  $L$  (m) and the distance between the corona wire and one of the collecting plates  $s$  (m), as well as the fluid and particle velocities.

## III. RESULTS AND DISCUSSION

The way to validate this model was to compare the distribution of the electric potential with the experimental results obtained by Penney [13]. For the validation, a simulation is considered under the following geometric parameters, a 0.15 mm corona wire radius, a distance between two corona wires is 150 mm, a width of 228.6 mm, and a length of 609.6 mm under conditions described in Table I. The numerical solution obtained corresponds with the experimental data shown in Fig. 5.

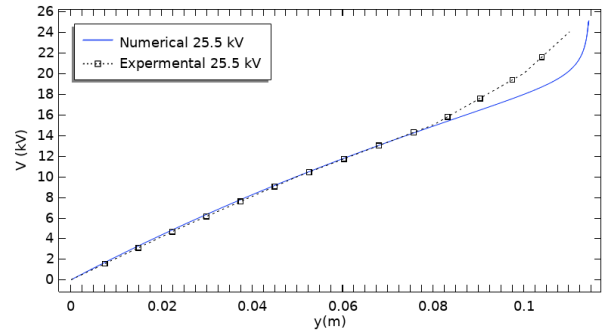


Fig. 5. Numerical simulation in comparison with Penney's experimental results, electrical potential distribution between the corona wire and collecting electrode.

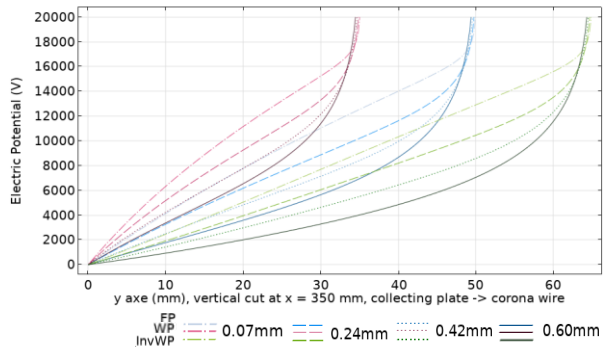


Fig. 6. Electric potential distribution using FPs, WPs, and InvWPs.

### A. Electrical Potential under Different Corona Wires

An electric potential of 20 kV is applied to the three corona wires, and the collecting plates are set to ground. In Fig. 6, the electric potential distribution is observed starting from one of the collecting plates into the border of the corona wire. The curves plotted correspond to the second corona wire for each case of FPs, WPs, and InvWPs.

Nevertheless, the higher distance between a collecting plate and the corona wire will be when InvWPs, and the shortest distance when WPs, because of their geometric arrangements. In a specific case, a more linear electric potential distribution is observed using FP and InvWPs with a corona wire radius of 0.07 mm than with the other corona wires. With a higher radius of corona wires, the potential is distributed at lower levels than with a smaller radius. The electric potential, in this case, increases faster as it approaches the corona wire. In fact, with this data a smaller corona wire radius can denote a more linear behavior.

### B. Electric Field Distribution under Different Corona Wires Radius

Taking as a principle that the electric field is inversely proportional to the distance between an electric potential difference, larger magnitudes of an electric field will be present in the case of WPs, and smaller magnitudes in the case of InvWPs. Due to the geometric shape of the collector plates, a horizontal cut is defined at  $y = 30$  mm; in Fig. 7, this distribution in magnitude is observed for FPs, WPs, and InvWPs using different corona wire sizes. The distribution of the electric field in WPs and FPs are similar with a faster growth and decrease in the proximity

of the corona wires. However, a particular case is observed in InvWPs with a corona wire radius of 0.007 mm, 0.24 mm, and 0.42 mm; the electric field is distributed in a much smaller vertical range (green lines).

In addition, lower values in magnitude occur when using InvWPs compared with FPs or WPs, FPs is the reference for the results obtained.

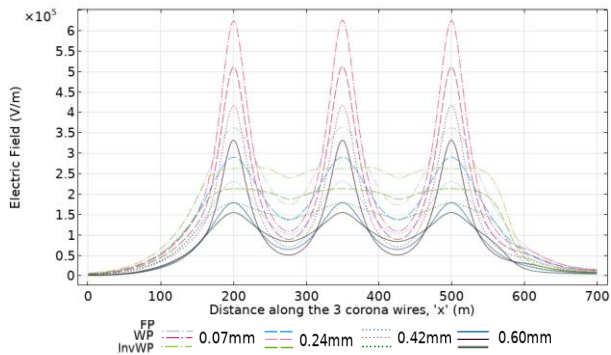


Fig. 7. Electric field distribution using FPs, WPs, and InvWPs.

### C. Current Density and Space Charge Density Distribution under Different Corona Wires Radius

Fig. 8 and Fig. 9 show the distribution of current density and charge space density respectively, both graphs show similar behavior. First, the current density is represented in a uniformly distributed way around each corona wire, the largest magnitudes are in the center of the corona wires, and the minimum values are in the midpoint between two corona wires. Using InvWPs the levels in the magnitude of current density are reduced a percentage over 50 percent if we compare with WPs. With smaller corona wire radius, the growth and decrease of these magnitudes in the vicinity of the corona wires are faster, and higher magnitude levels are also reached. The relationship between the current density and the corona wire radius is inverse, the same happens with the space charge density.

The space charge density is the solution of the mobility equation. In Fig. 9, this distribution is shown for the three collecting plate types; values in smaller magnitude are found between the two corona wires and the maximum in the center of the corona wires. Peek's law defines the space charge density at the corona wire surface values. However, in Fig. 9, these graphs are at  $y = 30$  mm to compare among the different collecting plate shapes.

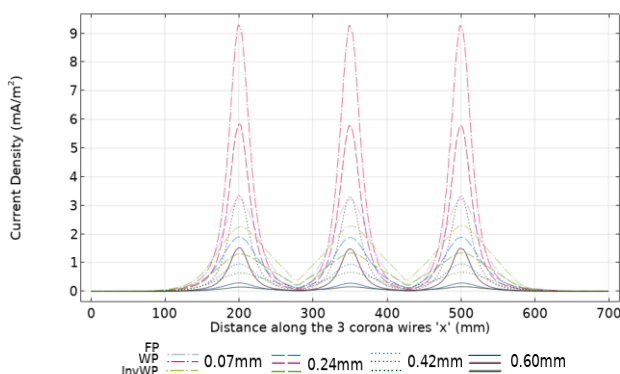


Fig. 8. Current density distribution using FPs, WPs, and InvWPs.

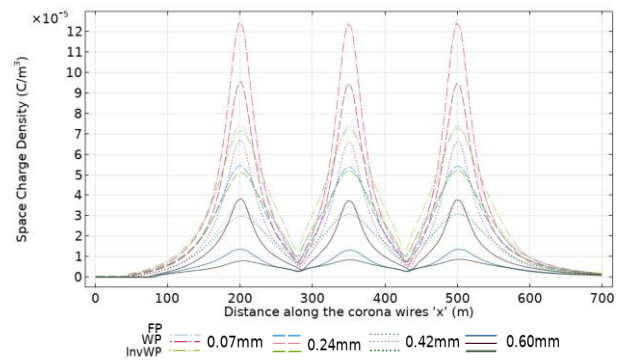


Fig. 9. Space charge density distribution using FPs, WPs, and InvWPs.

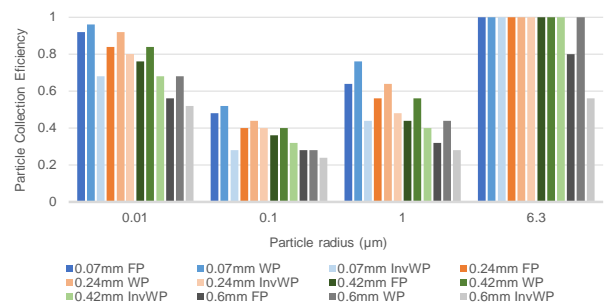


Fig. 10. Electric potential distribution using FPs, WPs, and InvWPs.

The reference point of this study is the use of FPs, comparing the use of WPs higher values in the magnitude of current density and space charge density are obtained, however, in the case of InvWPs, lower values are obtained for these magnitudes.

### D. Collection Efficiency

Fig. 10 shows the results obtained from particle collection efficiency when FPs, WPs, and InvWPs are used. FPs are the benchmark for evaluating WPs and InvWPs.

In Fig. 10, for corona wires radius of 0.07 mm, 0.24 mm, 0.42 mm, and 0.6 mm with WPs, higher particle collection efficiency levels are reached, and the lower levels with InvWPs. Nevertheless, a specific case is observed when InvWPs have a similar level of efficiency to FPs when particle radius is about 0.1  $\mu\text{m}$ ; however, overall, it will not justify the use of this geometric arrangement.

Using InvWPs reduce the levels of particle collection efficiency in the range of particle size shown in this study, in ranges of particle radius of 6  $\mu\text{m}$  lower levels of efficiency are observed compared when the other corona radius. Higher levels of efficiency are noted when using WPs and 0.07 mm corona wires.

## IV. CONCLUSION

This work proposed to observe the effect of inverting the wavy collecting plates to evaluate the electrical parameters when the radius of the corona wires is varied. The geometry of the WPs are referred to a study that shows higher degrees of efficiency using this geometric arrangement type. Therefore, it was proposed for InvWPs to use the exact dimensions as the WPs shown in this study. The results obtained using FPs were the reference

to define the following conclusions: The electric field is distributed more evenly when using InvWPs; this happens in a specific case when corona wires radius is 0.07 mm, 0.024 mm 0.42 mm. On the other hand, the behavior of the electric field shows a similar distribution for both FPs and WPs. Second, the relationship between space charge density and current density is inverse to the corona wires radius for all the types of collecting plates. Third: Using InvWPs, lower magnitudes of current density and space charge density are observed compared with FPs or WPs. Fourth: Using InvWPs does not improve the particle collection efficiency in a higher degree; there is a particular case (corona radius of 0.24 mm, particles of 0.1  $\mu\text{m}$ ) where a similar level to the FPs efficiency is observed. Finally, using WPs demonstrate the better performance of this geometry in this range of particles compared with InvWPs and FPs. InvWPs can be used to reduce the levels of current density or the space charge density, but it does not improve the collection efficiency. This provides a good starting point for discussion and further research. In future work, investigating different shapes of collecting plates especially wavy and inverted using different designs of corona wires such as needle wire might prove important.

#### CONFLICT OF INTEREST

The authors declare no conflict of interest.

#### AUTHOR CONTRIBUTIONS

Angel and Mo'ath conducted the research, wrote the paper, and analyzed the data. Tamás reviewed and made the corrections needed; all authors had approved the final version.

#### ACKNOWLEDGMENT

This work is supported by the Stipendium Hungaricum Scholarship.

#### REFERENCES

- [1] E. de Oliveira and V. G. Guerra, "Electrostatic precipitation of nanoparticles and submicron particles: Review of technological strategies," *Process Safety and Environmental Protection*, vol. 153, pp. 422–438, Sept. 2021.
- [2] Y. Zhuang, Y. J. Kim, T. G. Lee, and P. Biswas, "Experimental and theoretical studies of ultra-fine particle behavior in electrostatic precipitators," *J. Electrostat.*, vol. 48, no. 3–4, pp. 245–260, 2000.
- [3] A. Jaworek, A. Marchewicz, A. T. Sobczyk, A. Krupa, and T. Czech, "Two-stage electrostatic precipitators for the reduction of PM<sub>2.5</sub> particle emission," *Progress in Energy and Combustion Science*, vol. 67, pp. 206–233, July 2018.
- [4] G. Tu, Q. Song, and Q. Yao, "Experimental and numerical study of particle deposition on perforated plates in a hybrid electrostatic filter precipitator," *Powder Technology*, vol. 321, pp. 143–153, Nov. 2017.
- [5] X. Wang, "Effects of corona wire distribution on characteristics of electrostatic precipitator," *Powder Technology*, vol. 366, pp. 36–42, Apr. 2020.
- [6] L. Zhang, Y. Ninomiya, Q. Wang, and T. Yamashita, "Influence of woody biomass (cedar chip) addition on the emissions of PM<sub>10</sub> from pulverised coal combustion," *Fuel*, vol. 90, no. 1, pp. 77–86, 2011.
- [7] A. Jaworek, A. T. Sobczyk, A. Krupa, A. Marchewicz, T. Czech, and L. Śliwiński, "Hybrid electrostatic filtration systems for fly ash particles emission control. A review," *Separation and Purification Technology*, vol. 213, pp. 283–302, Apr. 2019.
- [8] G. H. Lee, S. Y. Hwang, T. W. Cheon, H. J. Kim, B. Han, and S. J. Yook, "Optimization of pipe-and-spike discharge electrode shape for improving electrostatic precipitator collection efficiency," *Powder Technology*, vol. 379, pp. 241–250, Feb. 2021.
- [9] M. Jędrusik, A. Świerczok, and A. Jaworek, "Collection of low resistivity fly ash in an electrostatic precipitator," *J. Phys. Conf. Ser.*, vol. 418, no. 1, 2013.
- [10] T.-Y. Wen, I. Krichtafovitch, and A. V. Mamishev, "Numerical study of electrostatic precipitators with novel particle-trapping mechanism," *Journal of Aerosol science*, vol. 95, pp. 95–103, May. 2016.
- [11] Y. Zhu, M. Gao, M. Chen, J. Shi, and W. Shangguan, "Numerical simulation of capture process of fine particles in electrostatic precipitators under consideration of electrohydrodynamics flow," *Powder Technology*, vol. 354, pp. 653–675, Sep. 2019.
- [12] H. Shen, W. Yu, H. Jia, and Y. Kang, "Electrohydrodynamic flows in electrostatic precipitator of five shaped collecting electrodes," *Journal of Electrostatics*, vol. 95, pp. 61–70, Oct. 2018.
- [13] W. Zhou, R. Jiang, Y. Sun, B. Chen, and B. Liu, "Study on multi-physical field characteristics of electrostatic precipitator with different collecting electrodes," *Powder Technology*, vol. 381, pp. 412–420, Mar. 2021.
- [14] H. Y. Choi, Y. G. Park, and M. Y. Ha, "Numerical simulation of the wavy collecting plate effects on the performance of an electrostatic precipitator," *Powder Technology*, vol. 382, pp. 232–243, Apr. 2021.
- [15] W. Gao, Y. Wang, H. Zhang, *et al.*, "Numerical simulation of particle migration in electrostatic precipitator with different electrode configurations," *Powder Technology*, vol. 361, pp. 238–247, Feb. 2020.
- [16] Y. Wang, W. Gao, H. Zhang, *et al.*, "Insights into the role of ionic wind in honeycomb electrostatic precipitators," *Journal of Aerosol Science*, vol. 133, pp. 83–95, Jul. 2019.
- [17] J. Wang, Y. Cai, X. Li, Y. Shi, and Y. Bao, "Electrically-induced ionic wind flow distribution and its application for LED cooling," *Applied Thermal Engineering*, vol. 138, pp. 346–353, Jun. 2018.
- [18] H. A. Said, M. Aissou, H. Nouri, and P. Y. Zebboudj, "Effect of wires number on corona discharge of an electrostatic precipitators," *Journal of Electrical Systems*, vol. 10, no. 4, pp. 392–405, 2014.
- [19] H. A. Said, H. Nouri, and Y. Zebboudj, "Analysis of current-voltage characteristics in the wires-to-planes geometry during corona discharge," *The European Physical Journal-Applied Physics*, vol. 67, no. 3, Sep. 2014.
- [20] U. Khaled and A. Z. Eldein, "Experimental study of V–I characteristics of wire–plate electrostatic precipitators under clean air conditions," *Journal of Electrostatics*, vol. 71, no. 3, pp. 228–234, 2013.
- [21] Y. Wang, H. Zhang, W. Gao, *et al.*, "Improving the removal of particles via electrostatic precipitator by optimizing the corona wire arrangement," *Powder Technology*, vol. 388, pp. 201–211, Aug. 2021.
- [22] A. Kasdi, "Computation and measurement of corona current density and V–I characteristics in wires-to-plates electrostatic precipitator," *Journal of Electrostatics*, vol. 81, pp. 1–8, June 2016.
- [23] E. Potrymai and I. Perstnov, "Time dependent modelling and simulation of the corona discharge in electrostatic precipitators," thesis, Dep. of Phys. and Elec. Eng., Linnaeus University, Sweden, 2014.
- [24] COMSOL Multiphysics. (2018). Electrostatic Precipitator. [Online]. Available: <https://www.comsol.com/model/electrostatic-precipitator-71361>

- [25] D. Rubineti, D. Weiss, and W. Egli, "Corona discharge—A fully coupled numerical approach verified and validated," *The International Journal of Multiphysics*, vol. 11, no. 4, pp. 375–386, 2017.
- [26] S. Li, Y. Huang, Q. Zheng, G. Deng, and K. Yan, "A numerical model for predicting particle collection efficiency of electrostatic precipitators," *Powder Technology*, vol. 347, pp. 170–178, Apr. 2019.

Copyright © 2022 by the authors. This is an open access article distributed under the Creative Commons Attribution License (CC BY-NC-ND 4.0), which permits use, distribution and reproduction in any medium, provided that the article is properly cited, the use is non-commercial and no modifications or adaptations are made.



**Angel G. Asipuella** was born in Ecuador in 1989. He was awarded a B.Sc. degree in electronics engineering from Army Polytechnic University, Quito, Ecuador, 2014. A M.Sc. degree in power electric engineering from Budapest University of Technology and Economics, Budapest, Hungary, 2018. He is currently preparing a Ph.D. degree at Budapest University of Technology and Economics, Budapest, Hungary. His main topic is focused with diagnostics and

modelling of electrostatics precipitators. He has been working in different areas such as electrical engineering in a power plant, electronics engineer in a forecasting research institution, and experience with supply chain.



**Mo'ath M. Bani Fayyad** was born on August 31<sup>st</sup>, 1990, in Irbid city, Jordan. He received a Bachelor of Science (B.Sc), in electrical power and machines engineering, from Yarmouk University, Jordan, in 2013. He completed his Master of Science (M.Sc.), in field of electrical power engineering, from Yarmouk University, in 2019. He is currently a Ph.D. student in electrical power engineering, at Budapest University of Technology and Economics, Budapest, Hungary. His research interests lie in the area of investigation of new technologies in electrostatic precipitators. He has four years of experience work in many fields, such as Quality Control Engineer at KADDB and Yarmouk University as Supervisor of Electrical Engineering Laboratories in the Department of electrical power engineering.



**Tamás Iváncsy** is an associate professor at the Budapest University of Technology and Economics, Department of Electric Power Engineering. He received a master's degree in electrical engineering and Ph. D. degree in electrical sciences from the Budapest University of Technology and Economics, Faculty of Electrical Engineering and Informatics.

His research field are electrostatics, electrostatic precipitation, power supplies for electrostatic precipitators and modelling of electrostatic precipitators. He is also interested in design of electric networks for buildings, nanogrid technology and building automation.